



Published in final edited form as:

J Nat Prod. 2020 July 24; 83(7): 2165–2177. doi:10.1021/acs.jnatprod.0c00257.

The Chemistry of Kratom [*Mitragyna speciosa*]: Updated Characterization Data and Methods to Elucidate Indole and Oxindole Alkaloids

Laura Flores-Bocanegra, Huzefa A. Raja, Tyler N. Graf, Mario Augustinovi, E. Diane Wallace, Shabnam Hematian, Joshua J. Kellogg, Daniel A. Todd, Nadja B. Cech, Nicholas H. Oberlies

University of North Carolina at Greensboro, Department of Chemistry and Biochemistry, Greensboro, NC 27402, United States

Abstract

Two separate commercial products of kratom [*Mitragyna speciosa* (Korth.) Havil. Rubiaceae] were used to generate reference standards of its indole and oxindole alkaloids. While kratom has been studied for over a century, the characterization data in the literature for many of the alkaloids are either incomplete or inconsistent with modern standards. As such, full ^1H and ^{13}C NMR spectra, along with HRESIMS and ECD data, are reported for alkaloids **1-19**. Of these, four new alkaloids (**7**, **11**, **17**, and **18**) were characterized using 2D NMR data, and the absolute configurations of **7**, **17**, and **18** were established by comparison of experimental and calculated ECD spectra. The absolute configuration for the *N*(4)-oxide (**11**) was established by comparison of NMR and ECD spectra of its reduced product with those for compound **7**. In total, 19 alkaloids were characterized, including: the indole alkaloid mitragynine (**1**) and its diastereoisomers speciociliatine (**2**), speciogynine (**3**) and mitraciliatine (**4**); the indole alkaloid paynantheine (**5**) and its diastereoisomers isopaynantheine (**6**) and epiallo-isopaynantheine (**7**); the *N*(4)-oxides mitragynine-*N*(4)-oxide (**8**), speciociliatine-*N*(4)-oxide (**9**), isopaynantheine-*N*(4)-oxide (**10**), and epiallo-isopaynantheine-*N*(4)-oxide (**11**); the 9-hydroxylated oxindole alkaloids speciofoline (**12**), isorotundifoline (**13**) and isospeciofoline (**14**); and the 9-unsubstituted oxindoles corynoxine A (**15**), corynoxine B (**16**), 3-epirhynchophylline (**17**), 3-epicorynoxine B (**18**), and corynoxine (**19**). With the ability to analyze the spectroscopic data of all of these compounds concomitantly, a decision tree was developed to differentiate these kratom alkaloids based on a few key chemical shifts in the ^1H and/or ^{13}C NMR spectra.

Graphical Abstract

Corresponding Author: Nicholas H. Oberlies – Department of Chemistry and Biochemistry, University of North Carolina at Greensboro; Nicholas_Oberlies@uncg.edu.

Supporting Information

The Supporting Information is available free of charge.

^1H NMR, ^{13}C NMR and HRESIMS data for compounds **1-19**. 2D NMR data (COSY, HSQC and HMBC) for new compounds **7**, **11**, **17** and **18**. ECD data for compounds **1-14** and **16-19**.



The scientific literature on the chemical composition of kratom [*Mitragyna speciosa* (Korth.) Havil. Rubiaceae] dates back nearly 100 years, when the most studied alkaloid from this plant, mitragynine (**1**), was reported in 1921.¹ The introduction to that paper concludes with the following prescient statements: “According to Redley.....*Mitragyne [sic] speciosa* is used in Perak against the opium habit, whilst, according to Dr. P.P. Laidlaw, mitragynine is a local anaesthetic, which finding is of interest, since the alkaloid contains an ester grouping.” At that time, there was uncertainty on the use of kratom. Interestingly, a century later, this uncertainty continues, including in the scientific literature, the popular press, and even government regulatory bodies. Many questions persist such as: *does kratom ameliorate pain? can it be used as an opioid substitute? does it relieve opioid withdrawal symptoms? does its use precipitate trips to the emergency room? is kratom harmful, harmless, or somewhere in between?* Addressing these questions requires a thorough understanding of the chemical composition of kratom.

In the past decade there has been an explosion in the biomedical literature regarding at least some of the above questions, particularly case reports (Figure S1). There are reports that speak to its ability to address pain, broadly defined.^{2–5} However, there are a similar number that suggest that it has opioid-like properties, and thus, may be an addiction liability.^{6–15} Towards that end, the US Food and Drug Administration has threatened to classify kratom as a schedule I controlled substance more than once, although at the writing of this paper, it has not done so.^{16–19}

As part of a project to study the potential for interactions between herbal medicines and drugs,^{20–24} our team was charged with generating reference standards of the kratom alkaloids. In doing so, we found many challenges and opportunities, largely due to gaps in the literature. Extensive chemical studies have been performed over the last century, resulting in the isolation of at least 54 alkaloids from the plant (see Figure S2), starting with the isolation of the main alkaloid, mitragynine (**1**), in 1921 by Ellen Field.¹ More than four decades later, and over a series of three manuscripts, Becket *et al.* and Zacharias *et al.* worked on the isolation, structure elucidation, and absolute configuration of **1**.^{25–27} Contemporaneously, the mitragynine diastereoisomers speciociliatine (**2**) and speciogynine (**3**) were reported.²⁸ A dozen years later, the fourth diastereoisomer, mitraciliatine (**4**), was

described from the leaves of *M. speciosa*.²⁹ Like many alkaloids, a majority of isolation studies on new compounds from kratom were carried out between the 1960s and 1980s.^{30–32} However, due to the growing popularity of this plant near the end of the last century, there was a renewed interest, resulting in the isolation of additional alkaloids (particularly minor constituents, which could be isolated due to advances in HPLC).^{33, 34} Despite this, most of the pharmacological studies on constituents from kratom have focused on mitragynine (**1**) and 7-hydroxymitragynine (see Figure S1). In general, the tetracyclic indole and pentacyclic oxindole alkaloids isolated from *M. speciosa* embody a few variations, that, collectively, show the interrelatedness of these compounds (see Figure S2). Some key motifs of the 54 known compounds from *M. speciosa* include a hydroxy or methoxy group at C-9, unsaturation at C-3, C-5 or C-18, hydroxylation at C-7, and various configurations at C-3, C-7 and/or C-20 (see Figure S2).^{30–32}

It was necessary to isolate standards for the alkaloids present in the plant, because even though there are over 50 kratom alkaloids reported, only 13 are commercially available (Figure S2). Moreover, in some cases we found that the quality of the commercial standards was not optimal, being mixtures, or were not even the correct compound.^{35, 36} From a pharmacological testing point of view, this is a serious problem, especially for scientists that don't have the training or collaborations to verify structural identity, as it could perpetuate erroneous findings in the literature. For these reasons, we strove to develop a series of reference standards, being able to isolate and characterize 19 kratom alkaloids (**1–19**), including four new analogues (**7**, **11**, **17**, and **18**). In doing so, we quickly realized that the reported spectroscopy data for some of the known compounds were limited, as is the case for many natural products.^{37–41} Thus, we took the opportunity to contribute by analyzing the NMR, HRESIMS, and ECD data for **1–19**, comparing the key differences between analogues.

RESULTS AND DISCUSSION

While there are some challenges associated with acquiring kratom plant material,⁴² two different sources could be obtained on the kg scale, which were termed 'Green Maeng Da' and 'White Jongkong' by the suppliers. These samples were slightly different in appearance, with the former being ground leaf fragments (internally coded as K49) and the latter being a fine powder (internally coded as K52) (see Figure S6). The taxonomy of these was examined using a combination of molecular methods, specifically DNA barcoding and maximum likelihood phylogenetic analysis. For the purpose of molecular identification, the most widely recommended loci were analyzed, including the plastid intergenic spacer *trnH-psbA*, *matK*, and the nuclear ribosomal internal transcribed spacer (ITS), since these three regions have been designated as the official DNA barcodes for the plant kingdom.^{43, 44} Of these, *trnH-psbA* is a widely used plastid marker, which displays a high rate of insertion and deletion and, as such, is widely used for plant barcoding studies.^{45–47} All three regions indicated that samples K49 and K52 could be unequivocally identified as *Mitragyna speciosa*. Maximum likelihood analysis of the partial *matK* region placed both commercial samples in a strongly supported clade (100% bootstrap support) with the published sequences for *M. speciosa* (Figure S3). Importantly, this analysis included a partial *matK* sequence from a recently sequenced genome of *M. speciosa* (BioProject: PRJNA325670). In

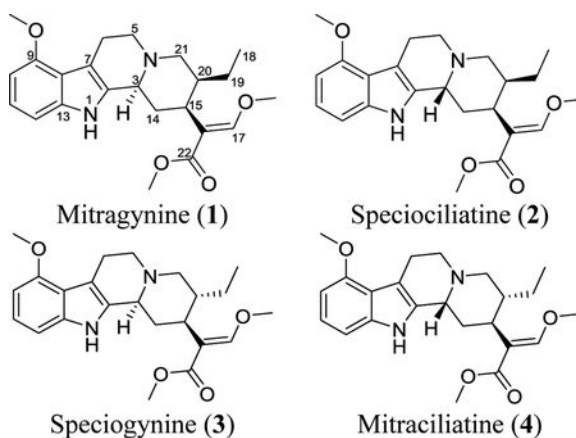
Author Manuscript

addition, a BLAST search of *matK* using the BOLDSYSTEMS database (version 4) showed that samples K49 and K52 had 99% sequence similarity with *M. speciosa* (Figures S4 and S5). As a confirmatory measure, maximum likelihood analysis using the ITS region also indicated that both samples formed a strongly supported clade (99% bootstrap support) with published sequence data of *M. speciosa* (Figure S6). Based on uncorrected p distances calculated for *trnH-psbA*, there was 99% sequence similarity with sequences of *M. speciosa*. This means that samples K49 and K52 were more similar to sequences of *M. speciosa* and more dissimilar to sequences of *M. diversifolia*, *M. hirsuta*, and *M. rotundifolia* (Tables S1 and S2). In short, three different methods all indicated that these materials were derived from *M. speciosa*. The sequence data were deposited in GenBank: *matK*: [MT114409](#) and [MT114408](#), *trnH-psbA*: [MT114410](#) and [MT114411](#), and ITS: [MT111840](#), [MT111841](#), [MT111842](#), and [MT111843](#).

Author Manuscript

Author Manuscript

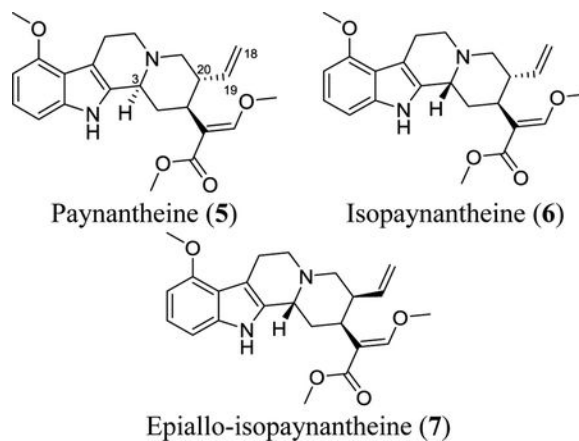
Even though the sources of kratom (i.e. K49 and K52) were demonstrated to be *M. speciosa* based on DNA barcoding, chromatographic profiles generated via UPLC-HRESIMS (Figure S7) showed clear differences in the profile of secondary metabolites. For instance, mitragynine (**1**) was the most abundant alkaloid in the K49 materials, while the K52 materials contained higher levels of speciofoline (**12**) and related alkaloids. While those differences may be somewhat surprising, varied chemical composition for different sources of *M. speciosa* has been documented, where plant age, environmental factors, and processing conditions impact on the suite of kratom alkaloids.^{48, 49} For example, in one published study the content of **1** derived from a Thai specimen was approximately five times higher than that derived from a Malaysian specimen.⁵⁰ Additionally, alkaloid differences between *M. speciosa* grown in Asia/Africa vs the United States have been noted.^{49, 51} Thus, for the purpose of generating structurally diverse kratom alkaloid reference standards, we selected sample K49 for the isolation of indole-type alkaloids and sample K52 for the isolation of oxindole-type alkaloids using an alkaloid partitioning scheme. The indole alkaloids mitragynine (**1**), speciociliatine (**2**), speciogynine (**3**), mitraciliatine (**4**), paynantheine (**5**),⁵² isopaynantheine (**6**)²⁹, epiallo-isopaynantheine (**7**), mitragynine-*N*(4)-oxide (**8**),⁵³ speciociliatine-*N*(4)-oxide (**9**),⁵³ isopaynantheine-*N*(4)-oxide (**10**),⁵⁴ and epiallo-isopaynantheine-*N*(4)-oxide **11** were isolated from the Green Maeng Da product (K49; see Figure S8), while the oxindole alkaloids speciofoline (**12**),⁵⁵ isorotundifoleine (**13**),⁵⁶ isospeciofoleine (**14**),⁵⁷ corynoxine A (**15**),^{58, 59} corynoxine B (**16**),⁵⁹ 3-epirhynchophylline (**17**), 3-epicorynoxine B (**18**), and corynoxine (**19**) were isolated from the White Jongkong product (K52; see Figure S9). Details for the structure elucidation for these compounds, including the identification of four new kratom alkaloids (i.e. **7**, **11**, **17**, and **18**) are presented below, using a suite of spectroscopic and spectrometric techniques (HRESIMS), including ECD. In doing so, a decision tree was developed that can be used to differentiate between these kratom alkaloids based on a few key signals in the ¹H and/or ¹³C NMR spectra (Figure 1). This flow diagram was designed to be helpful for those with only a limited understanding of structure elucidation, focusing on key signals that serve to differentiate between the various kratom alkaloid chemotypes.



Indole Alkaloids: Mitragynine (1) and Its Diastereoisomers (2–4).

Four diastereoisomers with a molecular formula of $C_{23}H_{30}N_2O_4$ were isolated, specifically mitragynine (1), speciociliatine (2), speciogynine (3), and mitraciliatine (4), all of which were verified via HRESIMS data, where the protonated molecule displayed m/z 399.2274, 399.2273, 399.2274, and 399.2275 ions, respectively (Figures S10–S13). While the absolute amounts likely vary in different kratom plant materials, the quantity of compound 1 isolated was at least 20 times greater than that for each of the other diastereoisomers (i.e. >450 mg of 1 vs ~20 mg of 2, 3, or 4). The 1H and ^{13}C NMR data matched with those reported previously,⁶⁰ and key characteristics included: 1) eight sp^2 signals in the ^{13}C NMR spectrum assignable to the indole moiety (C-2 and C-7 to C-13); 2) two doublets (δ_{H-10} 6.44–6.49 and δ_{H-12} 6.87–7.01) and one triplet (δ_{H-11} 6.99–7.07), all corresponding to the indole moiety; 3) signals for the vinylic proton at C-17 (δ_C/δ_H 160.2–160.7/7.32–7.44); 4) three methoxy groups attached to C-9, C-17, and C-22 (δ_C/δ_H 51.1–61.9/3.66–3.89); and 5) the methyl group at C-19 (δ_C/δ_H 11.1–13.0/0.74–0.89). Importantly, a thorough analysis of the differences between the characteristic signals permitted the unequivocal identification of compounds 1–4. For example, as Lee and colleagues described,⁶¹ when a deshielded proton singlet assignable to H-17 appeared at δ_H 7.43 or 7.44 (i.e. compounds 1 and 2, respectively), it was indicative of the α orientation of H-20. Alternatively, a more shielded chemical shift for H-17 (i.e. δ_H 7.32 and 7.35 for compounds 4 and 3, respectively), indicated the β orientation for H-20.⁶¹ Additionally, the orientation of H-20 could be confirmed orthogonally via the chemical shift of C-18, at δ_C of 12.5 or 13.0 (i.e. compounds 2 and 1, respectively) for the α orientation and δ_C of 11.1 (i.e. for both 3 and 4) for the β orientation. On the other hand, the presence of a broad singlet at δ_H 4.40 or 4.80 (i.e. compounds 2 and 4) agreed with the β orientation for H-3, but a signal at δ_H 3.20 or 3.21 (i.e. compounds 1 and 3) indicated the opposite orientation for the same proton (i.e., H-3 α). Indeed, the δ_{H-3} values of the α and β orientations depend on the dihedral angle and the distance between H-3 and the nitrogen lone pair. An anti-coplanar arrangement, as seen in the axial H-3 of the *trans* fused system in compounds 1 or 3 (i.e., α orientation), leads to shielding relative to the syn-coplanar arrangement of the equatorial proton (i.e., β orientation) in compounds 2 or 4, which have a dihedral angle of $\sim 60^\circ$ with the nitrogen lone pair. The donation of electron density into the antibonding orbital (i.e., $n \rightarrow \sigma^*$) of the axial C–H bond (i.e., α orientation) effectively results in the weakening of that bond and strong

shielding of the proton (Figure S18).^{62, 63} Key NMR signals for **1-4** are outlined (Table 1), and in addition, full 1D NMR spectra and Tables are reported in the Supporting Information (Figures S14–S17 and Table S4). Moreover, ECD spectra presented an additional approach for confirming the absolute configuration for these corynanthe-type alkaloids. It has been established that the Cotton effect between 250–300 nm could be used to establish the orientation of H-3, where a negative Cotton effect correlates with the β orientation (i.e., compounds **2** and **4**) and a positive Cotton effect for the α orientation for H-3 (i.e., compounds **1** and **3**; see Figure S19).⁶¹



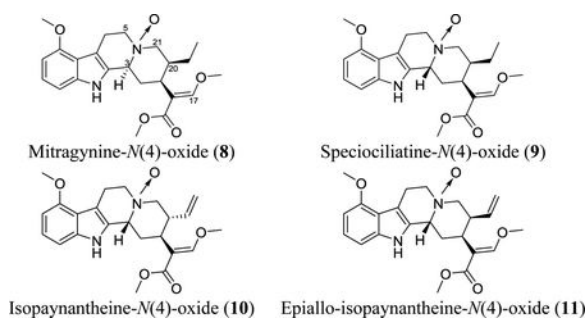
Indole Alkaloids: Paynantheine and Its Diastereoisomers (Compounds 5–7).

The structures of paynantheine (**5**) and isopaynantheine (**6**) were established by comparisons with literature data.⁵⁷ Their molecular formulae were confirmed by HRESIMS as $C_{23}H_{28}N_2O_4$, where the protonated molecule showed an m/z of 397.2119 and 397.2117, respectively (Figures S20 and S21). The NMR data of **5** and **6** resembled those for compounds **1-4**, sharing the previously enumerated characteristic signals for the indole ring. The main difference was the absence of signals for the C-20 ethyl moiety, and its replacement for a vinylic moiety, as evidenced by two doublets of doublets (δ_H 4.89–5.01) and a doublet of doublet of doublets or a doublet of triplets (δ_H 5.25–5.57), consistent with a 18(19) double bond (δ_{C-18} 115.7–116.7 and δ_{C-19} 137.9–139.4). As with **1-4**, the orientation of H-3 was deduced from chemical shift data, where the H-3 α orientation was noted for **5** (δ_H 3.20), while the more deshielded shift in **6** (δ_H 4.73) indicated the H-3 β orientation. These assignments were supported by the ECD spectra, where **5** and **6** had opposite Cotton effects at 250–300 nm. Specifically, a negative Cotton effect confirmed the β orientation (i.e. **6**) and a positive Cotton effect confirmed the α orientation (i.e. **5**) for H-3 (see Figure S32). Comparisons of the key NMR signals for compounds **5** and **6** are shown in Table 2, and the full 1D NMR spectroscopic data are reported in the Supporting Information (Figures S23–S24 and Table S5).

Compound **7** was isolated as an optically active yellow powder ($[\alpha]_D^{20} = +41.4$, c 0.1 $CHCl_3$), with a molecular formula of $C_{23}H_{28}N_2O_4$, deduced by HRESIMS, where the protonated molecule showed an m/z of 397.2115 (Figure S22). The 1H and ^{13}C NMR data of **7** resembled those of compounds **5** and **6**, sharing all the characteristic signals for an indole

alkaloid with 18(19) unsaturation (see Tables 2 and S5, and Figures S23–S25). These observations, along with differences in chromatographic retention times (**5**: 7.5 min, **6**: 7.0 min, and **7**: 9.0 min; see Figure S34), suggested that **7** was a new diastereoisomer of **5** and **6**. The HSQC data, along with COSY and HMBC correlations, were used to elucidate the structure of **7** (Figures S26–S28). For example, three isolated spin systems (specifically, H-10/H-11/H-12, H₂-5/H₂-6, and H-3/H₂-14/H-15/H-20/H₂-21/H-19/H₂-18) and key HMBC correlations (i.e. H-3 to C-2/C-7, H-17 to C-15/C-22, H₂-18 to C-20, CH₃O-9 to C-9, CH₃O-17 to C-17, and CH₃O-22 to C-22) were used to confirm the skeleton for the proposed structure (Figure 2).

To establish the absolute configuration of **7**, several complementary lines of reasoning were used. For instance, the deshielded signal at 4.85 ppm suggested H-3 β , since that was similar to the chemical shift for the same position in compounds **2** ($\delta_{\text{H-3}}$ 4.40), **4** ($\delta_{\text{H-3}}$ 4.80), and **6** ($\delta_{\text{H-3}}$ 4.73), all of which have been established to be H-3 β . Moreover, biogenetic assumptions were used for the C-15 configuration, since all the indole alkaloids from *M. speciosa* (42 compounds, to date) have the H-15 α orientation.³² Those considerations narrowed the possibilities for compound **7** to either the pseudo (i.e., 3 β , 15 α , and 20 β) or epiallo (i.e., 3 β , 15 α , and 20 α) orientation.⁶¹ The known compound, isopaynantheine (**6**), has the pseudo configuration, and thus, compound **7** is the 20-epimer of **6** (i.e. H-20 α), yielding an overall configuration of epiallo; those considerations were used to suggest the trivial name epiallo-isopaynantheine (**7**). In addition, ECD spectroscopy was used as an orthogonal probe of the proposed configuration. The spectrum for the epiallo configuration (i.e. 3 β , 15 α , and 20 α) was calculated using a time-dependent DFT (TDDFT) method at the B3LYP/6–31G+(d) level of theory, demonstrating concordance, including the aforementioned negative Cotton effect at ca. 275 nm that confirmed the H-3 β orientation (Figure 3). The NOESY spectra of compounds **6** and **7** were compared as well (Figures S29–S31). However, these data were inconclusive, since clear differences could not be discerned. This could be explained based on atomic distances, which were measured for the most stable conformers; in all cases these distances were < 5 Å (Figure S31). Collectively, the amalgamation of NMR and ECD data, and biogenetic considerations were used to establish the (3*R*,15*S*,20*S*) absolute configuration of the new indole alkaloid, epiallo-isopaynantheine (**7**).



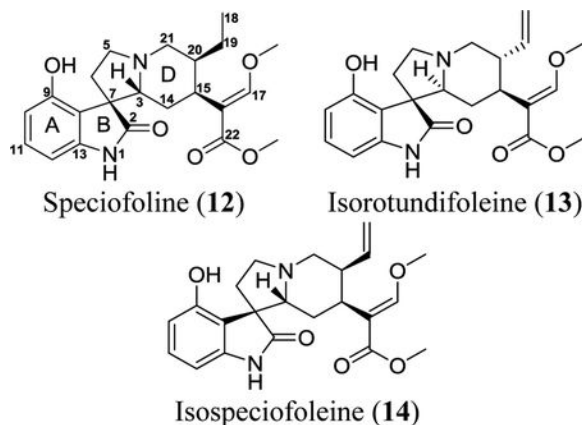
N(4)-oxides of Indole Alkaloids (8–11).

Compounds **8** and **9** had identical molecular formulae (C₂₃H₃₀N₂O₅), as determined by HRESIMS where the protonated molecules displayed an *m/z* of 415.2234 (**8**) and 415.2237

(9) (see Figure S35 and S36). This indicated that **8** and **9** had one extra oxygen atom compared to the diastereoisomers **1-4**. ^1H and ^{13}C NMR spectra of both had strong similarities with the spectroscopic data reported for mitragynine-*N*(4)-oxide, sharing the characteristic NMR signals for the *N*(4)-oxide indole alkaloids ($\delta_{\text{H-10}}$ 6.43, $\delta_{\text{H-11}}$ 6.99–7.03, $\delta_{\text{H-12}}$ 6.92–6.95, $\delta_{\text{C-17}}/\delta_{\text{H-17}}$ 161.3–161.5/7.45–7.46, $\delta_{\text{C-18}}/\delta_{\text{H-18}}$ 11.8–12.7/0.85–0.93, $\delta_{\text{C-21}}/\delta_{\text{H-21}}$ 68.5–68.6/3.53–3.72, $\delta_{\text{C-5}}/\delta_{\text{H-5}}$ 65.8–65.9/3.51–3.98, and three methoxy groups $\delta_{\text{C}}/\delta_{\text{H}}$ 51.6–62.1/3.61–3.86).³⁰ The main difference between the spectra for compounds **8** and **9**, relative to those discussed above for **1-4**, was deshielding of the signals attributed to H-3, H₂-5, and H₂-21, which was caused by a coordinate covalent bond in the *N*(4)-oxide group. There is an important distinction with the *N*-oxides, relative to the other kratom alkaloids, in that the $\delta_{\text{H-3}}$ value is small (~0.12 ppm) and does not correlate with the orientation of H-3. As noted in the discussion of **1-4**, the $\delta_{\text{H-3}}$ values of diastereoisomers mainly depend on the extent of interaction between the nitrogen free electron pair and the C–H antibonding orbitals. However, for the *N*-oxides, such an effect is not possible, since the electron pair is shared with the oxygen (i.e., N^+-O^- group). For the *N*-oxides, the positive charge on the nitrogen has a strong electron-withdrawing inductive effect, resulting in decreased electron density regardless whether the α -protons are axial or equatorial. In both compounds, the deshielded signal for the vinylic proton at $\delta_{\text{H-17}}$ 7.45–7.46 indicated the α orientation for H-20, analogous to compounds **1** and **2**. In addition, H-15 was presumed to have the α orientation, based on the biogenetic considerations discussed for compound **7**. Therefore, **8** and **9** could have the allo (i.e., 3 α , 15 α , and 20 α) or the epiallo (i.e., 3 β , 15 α , and 20 α) configurations. This illustrates another advantage of analyzing the ECD spectra of kratom alkaloids, particularly the Cotton effect at ca. 275 nm. Compounds **8** and **9** had opposite effects at ca. 275 nm, where a positive Cotton effect correlated with the H-3 α orientation (i.e. **8**) and a negative Cotton effect indicated the H-3 β orientation (i.e. **9**). In turn, these data allowed us to assign these compounds as mitragynine-*N*(4)-oxide (**8**)³⁰ and speciociliatine-*N*(4)-oxide (**9**). This is the first report of NMR characterization data for **9**, and key NMR signals for **8** and **9** are collated in Table 3, with full 1D NMR data reported in the Supporting Information (see Figures S39 and S40 and Table S6).

A similar set of observations were used to assign the structures of compounds **10** and **11**, which were isolated as orange powders with a molecular formula of $\text{C}_{23}\text{H}_{28}\text{N}_2\text{O}_5$ as calculated by HRESIMS via a protonated molecule with an m/z of 413.2079 (**10**) and 413.2077 (**11**) (Figures S37 and S38). For instance, the NMR data for **10** and **11** were similar to those reported for isopaynantheine-*N*(4)-oxide (Table 3). These NMR data also resembled those of **8** and **9**, where the main difference was the lack of the C-20 ethyl group (**10** and **11**) that was replaced with a vinylic group (see Table 3). In both cases, the signals for the vinylic proton appeared at $\delta_{\text{H-17}}$ 7.30–7.31, which was similar to the shifts in compounds **6** and **7**. Again, ECD data were helpful, where the negative Cotton effects between at ca. 275 nm correlated with the H-3 β orientation for both **10** and **11** (Figure S47). Additionally, a comparison of the ECD spectra of compounds **10** and **6** showed striking similarities; the same was true when comparing compounds **11** and **7** (see Figure S46). Therefore, compound **10** had the pseudo configuration (3 β , 15 α , and 20 β ; i.e., as seen in **6**) and **11** had the epiallo configuration (3 β , 15 α , and 20 α ; i.e., as seen in **7**). To confirm the absolute configuration of the new compound **11**, the method described by Shellard and

colleagues⁵³ was used. Briefly, **11** was reduced by addition of H₂SO₄, and the reaction product should correspond to the indole alkaloid without the oxide. Indeed, the ¹H NMR spectrum for the reduced product of **11** matched the spectrum of **7** (Figure S46). Collectively, these data permitted the characterization of these compounds as isopaynantheine-*N*(4)-oxide (**10**) and the new kratom alkaloid, epiallo-isopaynantheine-*N*(4)-oxide (**11**). The spectroscopic data for both are reported in the Supporting Information (Figures S41–S45 and Table S6).

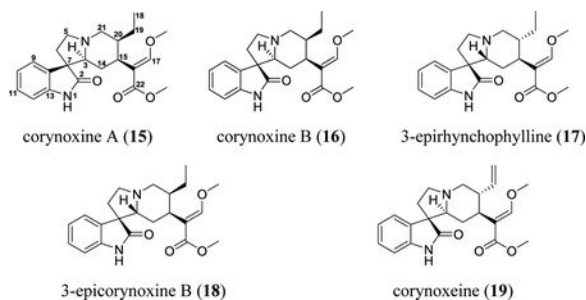


Oxindole Alkaloids: 9-Hydroxylated Oxindoles Like Speciofoleine (**12–14**).

Compound **12** had a molecular formula of C₂₂H₂₈N₂O₅, based on the protonated HRESIMS molecule with an *m/z* of 401.2067 (Figure S48). Comparison of the NMR data with key NMR signals in the ¹H and ¹³C spectra reported previously permitted the identification of this compound as speciofoleine (**12**) (Table 4).^{55, 56} This compound, which is one of the main alkaloids present in kratom (e.g. >55 mg isolated in this study), was first reported in 1963.⁵⁵ We have included the full spectroscopic data for **12** to serve as a reference point when analyzing the spectroscopic data for some of the more minor oxindole alkaloids. For instance, the C-ring (i.e., the pyrollidine ring) of **12** is connected to the γ -lactam (i.e., B-ring) through a C-7 spiro carbon, and this results in characteristic signals in the ¹³C NMR spectrum at δ_C 180.2 and 57.3 for the carbonyl in the oxindole ring and the spiro C-7 carbon, respectively (Table 4); the lactam signal, in particular, serves to quickly differentiate between indole and oxindole alkaloids (see Figure 1). Other important NMR signals, which are similar to those discussed above for the indole alkaloids, include: 1) signals for the indole system (δ_{H-10} 6.35, δ_{H-11} 7.05 and δ_{H-12} 6.53); 2) a vinylic H-17 (δ_C/δ_H 159.8/7.38); 3) two methoxy groups at C-17 and C-22 (δ_C/δ_H 61.3/3.79 and δ_C/δ_H 51.7/3.65, respectively), and 4) a methyl group ($\delta_{C-18}/\delta_{H-18}$ 12.3/0.83). Key NMR signals for **12** are tabulated (Table 4), and the full 1D NMR spectroscopic data are reported in the Supporting Information (Figure S51 and Table S7).

Additionally, two other 9-hydroxylated oxindole alkaloids were isolated and characterized as isorotundifoleine (**13**) and isospeciofoleine (**14**). The molecular formula for both isomers was C₂₂H₂₆N₂O₅ as measured by HRESIMS based on protonated molecules with *m/z* values of 399.1909 and 399.1906, respectively (Figures S49 and S50). The structures were elucidated by comparing the NMR data with those reported previously (Table 4),^{56, 57} and

the full assignment of the ^1H and ^{13}C NMR spectroscopic data for both are reported in the Supporting Information (Figures S52 and S53, and Table S7); this is the first report of comprehensive NMR data for **13**. The NMR data for both **13** and **14** resembled those described above for speciofoline (**12**), with a major difference being the absence of the methyl group (i.e., C-18 in **12** at $\delta_{\text{C}}/\delta_{\text{H}}$ 12.3/0.83), which was replaced by the 18(19) double bond ($\delta_{\text{C}}/\delta_{\text{H}}$ 116.4/4.95–5.01 and $\delta_{\text{C}}/\delta_{\text{H}}$ 138.6–138.8/5.43–5.49, respectively, for **13** and **14**). As with the indole alkaloids, ECD spectra were instrumental in assigning the configuration of these compounds, especially for analyzing the C-7 spiro center. According to the literature, the negative Cotton effect at 290 nm confirmed the (7*R*) configuration in compounds **12** and **13**, and the positive Cotton effect agreed with the (7*S*) configuration in compound **14**. Additionally, the negative Cotton effect around 250 nm confirmed the H-3 β orientation in compounds **12** and **14**, whereas the opposite Cotton effect demonstrated the H-3 α orientation in **13**. These results agreed with the rules for ECD spectra for the 9-hydroxylated oxindole alkaloids, and a calculated ECD spectrum was generated for **12** as a confirmatory measure (see Figure S54).^{56, 64}



Oxindole Alkaloids: 9-Unsubstituted Oxindoles Such as Corynoxine A (15–19).

Two closely related isomers, **15** and **16**, were isolated with a molecular formula of $\text{C}_{22}\text{H}_{28}\text{N}_2\text{O}_4$, based on HRESIMS protonated molecules with m/z values of 385.2119 (i.e. **15**) and 385.2127 (i.e. **16**) (Figures S55 and S56). The compounds were characterized using ^1H and ^{13}C NMR data as corynoxine A (**15**) and corynoxine B (**16**), based on concordance with published data for synthetic standards of these compounds (Tables 5 and S8 and Figures S60 and S61).⁶⁵ In addition, the NMR data for **15** and **16** resembled those described for **12**, with the main difference being replacement of the C-9 phenolic group with an aromatic proton, which resulted in a pattern of two doublets and two triplets of doublets for the protons in the oxindole ring (H-9 to H-12, see Table 5). Both **15** and **16** had the allo configuration (i.e., 3 α , 15 α , and 20 α), with opposite configurations at the spiro C-7, being (7*S*) for **15** and (7*R*) for **16**. As Trager and colleagues reported,⁶⁴ the configuration at C-7 can be deduced based on the chemical shift for the H-9 signal. For instance, when presuming the allo configuration, the presence of a deshielded signal for H-9 (δ_{H} 7.45) confirmed the (7*S*) configuration for **15** and the (7*R*) configuration in **16** due to the more shielded signal for H-9 (δ_{H} 7.19). While **15** was stable, an interesting challenge with compound **16** was its interconversion to **15** over a period of about 8 days in CDCl_3 (see Figure S62). As reported previously,⁶⁶ the epimerization process increases under acidic conditions via an intermolecular Mannich reaction, resulting in a ratio of ~70:30 of **15** and **16**, respectively (see Figure S62). As such, only the ECD spectrum of **15** is reported, supporting the (7*S*) and

the allo configurations based on negative Cotton effects around 290 nm and 250 nm (Figure S76).

Compounds **17** and **18** were isolated as optically active powders ($[\alpha]_D^{23} -30$ (c 0.1, CHCl_3) and $[\alpha]_D^{24} -46$ (c 0.1, CHCl_3), respectively). Their molecular formulae were established as $\text{C}_{22}\text{H}_{28}\text{N}_2\text{O}_4$ based on the HRESIMS protonated molecule with m/z values of 385.2119 (i.e. **17**) and 385.2120 (i.e. **18**) (Figures S57 and S58). The ^1H and ^{13}C NMR spectra of these compounds were similar to those of **15** and **16** (Table 5). These data, along with their different retention times (**17**: 2.76 min and **18**: 2.87 min) (see Figures S57 and S58), suggested that **17** and **18** were new isomers of **15** and **16**. The HSQC data, along with COSY and HMBC correlations, were used to confirm the proposed structures. In both cases, three isolated spin systems (specifically H-9/H-10/H-11/H-12, H₂-5/H₂-6, and H-3/H₂-14/H-15/H-20/H₂-21/H₂-19/H₃-18) and key HMBC correlations (i.e. H-3 to C-2/C-7, H-17 to C-15/C-22, H₃-18 to C-20, CH_3O -17 to C-17, and CH_3O -22 to C-22) were used to confirm the 2D structures of **17** and **18** (see Figures 2 and S63–S65 and S69–S71). Similar to the discussion for **6** and **7**, the correlations observed in the NOESY spectra for **17** and **18** were not useful to determine the relative configuration for these compounds (Figures S67 and S73). The absolute configuration of these molecules was proposed based on ECD experiments, following the rules described for the 9-unsubstituted oxindole alkaloids. In particular, the related isomer rhynchophylline served as a reference, since the crystal structure for this compound has been published and the ECD data were well described.^{64, 67} For instance, both **17** and **18** had the (7*R*) configuration, based on positive Cotton effects around 290 nm, and the H-3 β orientation, as noted by positive Cotton effects around 250 nm (Figure S76). Using biogenetic reasoning for the H-15 α orientation, along with the evidence observed in the ECD data, we deduced that compounds **17** and **18** should have the pseudo (i.e., 3 β , 15 α , and 20 β) or epiallo (i.e., 3 β , 15 α , and 20 α) configurations. To evaluate that presumption, the ECD spectra for the diastereoisomers at C-20 were calculated using a time-dependent DFT (TDDFT) method at the B3LYP/6–31G+(d) level of theory. The results showed that the calculated ECD spectrum for H-20 β matched with the ECD spectrum for **17**, and similarly, the calculated ECD spectrum for an analogue with the H-20 α orientation matched with the ECD spectrum for compound **18** (Figure 4). NMR data, biogenetic considerations, and the examination of ECD spectra were used to establish the absolute configuration of the new oxindole alkaloids, (3*R*,7*R*,15*S*,20*R*)-3-epirhynchophylline (**17**) and (3*R*,7*R*,15*S*,20*S*)-3-epicorynoxine B (**18**).

Compound (**19**) was isolated as a white powder, and its molecular formula was established as $\text{C}_{22}\text{H}_{26}\text{N}_2\text{O}_4$, based on the HRESIMS protonated molecule with an m/z of 383.1964 (Figure S59). The NMR data for this compound showed strong similarities with the data of **15–18**, where the main differences were the absence of the signals for the C-20 ethyl group, which was replaced by a vinylic group (Tables 5 and S8). The NMR data (Figure S75 and Table S8) matched with those reported for corynoxine.⁶⁸ ECD data corroborated the H-3 α orientation based on the negative Cotton effect around 250 nm, and the (7*R*) configuration based on the positive Cotton effect around 290 (Figure S76).

To add complementary data to the structural characterization of the kratom alkaloids, an attempt was made to analyze compounds **1**, **6**, **7**, **15**, **17**, and **18** by VCD, so as to examine a range of both indole and oxindole alkaloids. However, in all cases the similarities between calculated and experimental data were low, ranging between 57.7 to 70.0% (Table S9). In contrast, prominent recent VCD results published in this *Journal* report similarities ranging between 74.1 to 98.5%.^{69–73} In particular, we were surprised at the lack of concordance with the data for mitragynine (**1**), since it has been so well characterized, including by X-ray crystallography.²⁷ Thus, the purity of **1**, **6**, **7**, **15**, **17**, and **18**, were examined after the completion of the VCD studies, and indeed, it was obvious that the compounds decomposed during the experiments (see Figure S77). Based on the ¹H NMR spectra (data not shown), we hypothesize that epimers were formed, likely as a result of the VCD data being recorded at elevated temperatures in CHCl₃ for up to 18 hours; the epimerization potential of these compounds has been reported.⁶⁶ While disappointing, we determined that analysis of VCD spectra is not helpful for this class of compounds, at least with current technologies, due to their lack of stability under the analytical conditions.

In summary, 19 reference standards were isolated from kratom plant materials, including the two new indole alkaloids **7** and **11** and the two new oxindole alkaloids **17** and **18**. To characterize their structures, including absolute configuration, a combination of mass spectrometry and NMR and ECD spectroscopy were utilized. An added benefit of analyzing the NMR spectroscopy data for a suite of closely related compounds was that it facilitated the development of a decision tree (Figure 1). Using only a few key NMR signals, even a relative novice should be able to narrow the possible structures for at least these kratom alkaloids, and an expert is encouraged to examine a full suite of NMR data in relation to those reported in the Supporting Information. It is our hope that improvements in the structural characterization of the kratom alkaloids will result in more clarity in the biomedical literature on this interesting class of compounds.

EXPERIMENTAL SECTION

General Experimental Procedures.

Optical rotations were obtained in CHCl₃ using a Rudolph Research Autopol III polarimeter. UV and ECD spectra were acquired on a Varian Cary 100 Bio UV-Vis spectrophotometer and an Olis DSM 17 CD spectrophotometer (Olis), respectively. A ChiralIR-2X dual-source, dual-polarization-modulated FT-VCD spectrometer was used to carry out IR and VCD measurements. NMR experiments were conducted using either a JEOL ECA-500 NMR spectrometer operating at 500 MHz for ¹H and 125 MHz for ¹³C or a JEOL ECS-400 NMR spectrometer equipped with a high sensitivity JEOL Royal probe operating at 400 MHz for ¹H and 100 MHz for ¹³C; the residual solvent signals were utilized for referencing. HRESIMS was performed on a Thermo LTQ Orbitrap XL mass spectrometer equipped with an electrospray ionization source. UPLC was carried out on a Waters Acquity system with data collected and analyzed using Thermo Xcalibur software. HPLC was carried out using a Varian ProStar HPLC system equipped with ProStar 210 pumps and a ProStar 335 photodiode array detector (PDA), with data collected and analyzed using Galaxie Chromatography Workstation software (version 1.9.3.2). For preparative HPLC, a series of

Phenomenex columns were used, including a Kinetex C₁₈ (5 μm; 250 × 21.2 mm), a Luna CN (5 μm; 250 × 21.2 mm) and a Luna PFP (5 μm; 250 × 21.2 mm) all at a 20 mL/min flow rate. For UPLC, a Waters BEH C₁₈ column (1.7 μm; 50 × 2.1 mm) was used with a 0.6 mL/min flow rate. Flash chromatography was performed on a Teledyne ISCO CombiFlash Rf 200 using various sizes of Silica Gold columns and monitored by UV and evaporative light-scattering detectors.

Plant Material, DNA Extraction, PCR and Sequencing for Molecular Identification.

The commercial kratom products used to prepare extracts [i.e. Green Maeng Da (K49, batch: M-1005, 4 kg) and White Jongkong (K52, batch: BN-1006, 1 kg)] were identified by DNA barcoding. The manufacturers reported these as both from Southeast Asia, with K49 being chipped leaf materials and K52 being a fine powder. Samples were handled using methods described previously for the DNA barcoding of commercial mushroom products.⁷⁴ Briefly, one scintillation vial was made from each product (see Figure S6), where the vial was filled with plant material from the top and middle layers of the commercial product, and these were labeled with product name, lot number, and batch number and stored at ambient temperature in a bench drawer. For DNA extractions, approximately 5 mg of plant powder was taken from the scintillation vial and transferred to a bashing bead tube with DNA lysis buffer provided by Zymo Research Quick-DNA plant/seed miniprep DNA extraction kit. DNA was extracted using procedures outlined in the Zymo Research plant DNA extraction kit. The plastid gene *matK* was PCR amplified with primer combination *matK-xf* and *matK-MALP*;^{75, 76} for *psbA-trnH* primer combination *psbA – trnH*,⁷⁷ and for nuclear ITS, primer combination ITS-u1 and ITS-u4⁷⁸ was used for PCR and sequencing. All PCRs were amplified on an Applied Biosystems Veriti thermal cycler using PuReTaq Ready-To-Go PCR Beads (GE Healthcare) with the above primers. The PCR reaction was carried out in 25 μL containing 5 μL template DNA, 2.5 μL BSA, 2.5 μL 50% DMSO, and 1 μL of each forward and reverse primer at a concentration of 10 μM. The rest of the volume was made up to 25 μL by adding molecular biology grade water from Fisher Scientific. PCR thermocycler parameters for all fragments are outlined (Table S3). The PCR products were then run on an ethidium bromide-stained 1% agarose gel (Fisher Scientific) along with a 1 kb DNA ladder (Promega) to estimate the size of the amplified band. PCR products were purified using a Wizard SV Gel and PCR Clean-up System. Sanger sequencing of the purified PCR products was performed at Eurofins Genomics (<http://www.operon.com/default.aspx>) using BigDye Terminator v3.1 cycle sequencing. The sequencing was accomplished bidirectionally using both strands with the same primers used for the PCR amplification. Sequences were generated on an Applied Biosystems 3730XL high-throughput capillary sequencer. For both sequencing reactions, approximately 15 μL of PCR template was used along with 2 μM sequencing primers. Sequences were assembled with Sequencher 5.3 (Gene Codes), optimized, and then corrected manually when necessary; the latter step was to ensure that the computer algorithm was assigning proper base calls. Each sequence fragment was subjected to an individual NCBI GenBank, Basic Local Alignment Search Tool (BLAST) search as well as the BOLDSYSTEMS database to verify identity.

BLAST Search and DNA Barcoding.—For identification of kratom plant material via DNA Barcoding, one plastid region (*matK*) was utilized for plant identification by BLAST

searching against the BOLDSYSTEMS database version 4. In addition, the sequences of *matK* were compared against an authentic partial sequence of *matK* from the *Mitragyna speciosa* genome assembly (Center for Food Safety and Applied Nutrition (CFSAN), part of the USDA). Uncorrected p-distances were calculated in Geneious, a bioinformatics desktop software package (<http://www.biomatters.com>), for sequences obtained from the *psbA-trnH* plastid region, which is considered as one of the most variable regions of angiosperm plants, as well as for nuclear ITS region for the published sequence data from GenBank for *Mitragyna* spp.^{79–81} including *M. speciosa* and the newly obtained sequences in this study. The p-distances were obtained by dividing the number of nucleotide differences by the total number of nucleotides being compared. An arbitrary cut off proxy of 98–100% was applied as a criterion to designate similar species; therefore, to be considered the same species based on *psbA-trnH* and ITS sequence comparison, the taxa being compared would have 98% sequence similarity.

Molecular Phylogenetic Analysis.—Maximum likelihood analysis was performed separately for both the nuclear ITS and the plastid *matK* region to place the kratom samples into a phylogenetic framework with published sequences of *M. speciosa*. Methods for maximum likelihood analysis have been outlined previously.⁸² *Nauclea officinalis* (Rubiaceae) was used as an outgroup taxon in both nuclear ITS and *matK* analyses.

Extraction and Isolation of Kratom Alkaloids from Green Maeng Da.

The kratom plant material (Green Maeng Da, 4 kg; Figure S8) was extracted with 10 L of CHCl₃-CH₃OH (1:1) and 500 mL of 10% aqueous KOH by maceration over 24 h at room temperature. The mixture was filtered, and the solvent was evaporated under reduced pressure. The dried extract was reconstituted in a solution of 1M HCl and hexanes (1:1), transferred into a separatory funnel, and shaken vigorously. The hexanes phase was drawn off, the pH of the aqueous phase was adjusted to 9.0 with dropwise addition of concentrated NH₄OH, and the alkaloids were extracted as the free base with CHCl₃; after washing with neutral water, the organic phase was dried to yield 12 g of the alkaloid extract. This material was fractionated by normal phase flash chromatography using a silica column (120 g) and a gradient solvent system of hexanes-CHCl₃-CH₃OH at a flow rate of 85 mL/min over 67 min to yield 11 pooled fractions.

Fraction 4 (500 mg) was subjected to reverse phase HPLC using a CN column and a gradient system of 40:60 to 100:0 of CH₃OH-H₂O (10 mM of NH₄OAc in both phases) over 20 min with a flow rate of 20 mL/min. This process yielded eight subfractions, and fraction 8 was identified as compound **1** (450.5 mg).

Fraction 9 (1.1 g) was fractionated by normal phase flash chromatography using a silica column (12 g) and a gradient system of hexanes-EtOAc-CH₃OH using a flow rate of 30 mL/min to generate four subfractions. Subfraction 2 (40 mg) was purified by preparative HPLC over a CN column using a gradient of 70:30 to 100:0 of CH₃OH-H₂O (10 mM of NH₄OAc in both phases) over 20 min with a flow rate of 20 mL/min. This process yielded compounds **4** (13.1 mg) and **6** (15.20 mg). Subfraction 4 (800 mg) was subjected to flash chromatography using a silica column (12 g) via a gradient of CHCl₃-CH₃OH (10 mM of

NH₄OAc in both phases) over 60 min with a flow rate of 30 mL/min to generate five fractions (F9-4_1 through F9-4_5). Fraction F9-4_3 was subjected to preparative HPLC over a Kinetex column using a gradient of 60:40 to 70:30 of CH₃OH-H₂O (10 mM of NH₄OAc in both phases) over 30 min with a flow rate of 20 mL/min; three fractions were collected and the first fraction was characterized as compound **2** (20.5 mg). Fraction F9-4_4 (300 mg) was subjected to flash chromatography using a silica column (4 g) and a gradient of hexanes-acetone-CH₃OH over 20 min at a flow rate of 18 mL/min to generate eight fractions. The second fraction was resolved by preparative HPLC over a CN column using a gradient of 50:50 to 100:0 of CH₃OH-H₂O (10 mM of NH₄OAc in both phases) over 20 min with a flow rate of 20 mL/min; this process yielded 16.5 mg of compound **7**. The seventh fraction (16 mg) from F9-4_4 was subjected to preparative HPLC using a CN column and a gradient of 40:60 to 90:10 of CH₃OH-H₂O (10 mM of NH₄OAc in both phases) over 20 min with a flow rate of 20 mL/min; two fractions were collected and the first fraction was characterized as compound **11** (2.3 mg). Fraction F9-4_5 (40 mg) was subjected to preparative HPLC over a Kinetex column with a gradient of 50:50 to 100:0 of CH₃OH-H₂O (10 mM of NH₄OAc in both phases) over 35 min with a flow rate of 20 mL/min; the third fraction was identified as **8** (10.5 mg).

Fraction 6 (680 mg) was subjected to a second fractionation using flash chromatography over a silica column (12 g) and a gradient of CHCl₃-CH₃OH (10 mM of NH₄OAc in both phases) over 60 min with a flow rate of 30 mL/min to generate five subfractions. Subfraction 1 (47 mg) was subjected to preparative HPLC over a CN column and a gradient system of 55:45 to 100:0 CH₃OH-H₂O (10 mM of NH₄OAc in both phases) over 25 min; the first and second fractions were identified as **5** (9.83 mg) and **3** (18.33 mg), respectively.

Fraction 8 (1.3 g) was fractionated by flash chromatography using a silica column (12 g) with a gradient of CHCl₃-CH₃OH (10 mM of NH₄OAc in both phases) over 25 min with a flow rate of 30 mL/min to generate four subfractions. Subfractions 3 (12.8 mg) and 4 (7.0 mg) were purified by preparative HPLC over a CN column and a gradient system of 50:50 to 100:0 CH₃OH-H₂O (10 mM of NH₄OAc in both phases) over 15 min at a flow rate of 20 mL/min to yield compounds **9** (5.7 mg) and **10** (4.5 mg), respectively.

Extraction and Isolation of Kratom Alkaloids from White Jongkong.

The plant material (White Jongkong, 1 kg; Figure S9) was extracted exhaustively using the same procedure described above, to obtain 1.0 g of the dried extract. Normal phase flash chromatography was used to separate the extract using a silica column (24 g) and a gradient system of hexanes-CHCl₃-CH₃OH over 52 min at a flow rate of 35 mL/min to generate 13 fractions. Fractions 3 (100.0 mg) and 4 (80.0 mg) were purified, separately, by preparative HPLC using a PFP column and a gradient of 70:30 to 100:0 CH₃OH-H₂O (10 mM of NH₄OAc in both phases) over 20 min at a flow rate of 20 mL/min to yield 38.2 mg of **15** (from fraction 3), and separately, 52.5 mg of **16** and 3.5 mg of **13** (from fraction 4).

Fraction 5 (80.5 mg) was subjected to preparative HPLC over a PFP column using a gradient of 70:30 to 100:0 CH₃OH-H₂O (10 mM of NH₄OAc in both phases) over 20 min at a flow rate of 20 mL/min to generate nine subfractions, and subfraction 4 was identified as compound **12** (55.0 mg).

Fractions 6 (156.2 mg) and 7 (84.1 mg) were combined based upon their similar HPLC chromatographic profiles. The resulting fraction (240.3 mg) was resolved by flash chromatography over a silica column (12 g) using a gradient of hexanes-CHCl₃-CH₃OH over 25 min at a flow rate of 18 mL/min to generate eleven subfractions. Subfraction 2 (10.0 mg) was subjected to semipreparative HPLC over a PFP column using a gradient of 50:50 to 100:0 CH₃OH-H₂O (10 mM of NH₄OAc in both phases) over 20 min at a flow rate of 4.0 mL/min, yielding **17** (2.0 mg). Subfraction 4 (15.0 mg) was subjected to preparative HPLC over a PFP column using a gradient of 60:40 to 100:0 CH₃OH-H₂O (10 mM of NH₄OAc in both phases) over 20 min at a flow rate of 20.0 mL/min, yielding **14** (3.6 mg). Subfraction 5 (13.0 mg) was subjected to preparative HPLC over a PFP column using a gradient of 50:50 to 100:0 CH₃OH-H₂O (10 mM of NH₄OAc in both phases) over 20 min at a flow rate of 20.0 mL/min to generate four subfractions, where subfractions 2 and 3 were identified as **19** (1.7 mg) and **18** (1.1 mg), respectively.

Epiallo-isopaynantheine (7): Yellowish solid powder. $[\alpha]_D^{20} +41$ (*c* 0.1, CHCl₃); UV (CH₃OH) λ_{\max} (log ϵ) 233 (3.7), 339 (2.9) nm; ¹H and ¹³C NMR see Table 2 and Table S5; HRESIMS *m/z* 397.2115 [M + H]⁺ (calcd for C₂₃H₂₉N₂O₄, 397.2127).

Epiallo-isopaynantheine-N(4)-oxide (11): Orange powder. $[\alpha]_D^{23} +33$ (*c* 0.1, CHCl₃); UV (CH₃OH) λ_{\max} (log ϵ) 219 (3.2), 244 (3.9) nm; ¹H and ¹³C NMR see Table 3 and Table S6; HRESIMS *m/z* 413.2077 [M + H]⁺ (calcd for C₂₃H₂₉N₂O₅, 413.2076).

3-Epirhyncophylline (17): White powder. $[\alpha]_D^{23} -30$ (*c* 0.1, CHCl₃); UV (CH₃OH) λ_{\max} (log ϵ) 219 (3.3), 244 (3.6) nm; ¹H and ¹³C NMR see Table 5 and Table S8; HRESIMS *m/z* 385.2119 [M + H]⁺ (calcd for C₂₂H₂₉N₂O₄, 385.2127).

3-Epicorynoxine B (18): White powder. $[\alpha]_D^{24} -46$ (*c* 0.1, CHCl₃); UV (CH₃OH) λ_{\max} (log ϵ) 217 (3.4), 246 (3.7) nm; ¹H and ¹³C NMR see Table 5 and Table S8; HRESIMS *m/z* 385.2120 [M + H]⁺ (calcd for C₂₂H₂₉N₂O₄, 385.2127).

Computational Methods.

The minimum energy structures were built with Spartan'10 software (Wavefunction Inc., Irvine, CA, USA). The conformational analysis was performed using the Monte Carlo search protocol under the MMFF94 molecular mechanics force field.

For the ECD prediction, the resulting conformers were minimized using the DFT method at the B3LYP/6-311G+(2d,p) level of theory. Then, the time-dependent DFT (TDDFT) method at the B3LYP/6-31G+(d) level of theory was employed for ECD calculations. The calculated excitation energy (nm) and rotatory strength (R) in dipole velocity (Rvel) and dipole length (Rlen) forms were simulated into an ECD curve. All calculations were performed employing the Gaussian'09 program package (Gaussian Inc., Wallingford, CT, USA).

Supplementary Material

Refer to Web version on PubMed Central for supplementary material.

ACKNOWLEDGMENTS

This project was supported by the National Institutes of Health/National Center for Complementary and Integrative Health via the Center of Excellence for Natural Product Drug Interaction Research (NaPDI Center, U54 AT008909), including an Administrative Supplement for Validation Studies of Analytical Methods for Dietary Supplements and Natural Products. We thank our colleagues from UNC Greensboro (S. Knowles, Z. Al Subeh, and K. Cank) for evaluating the NMR decision tree.

REFERENCES

- (1). Field E J. Chem. Soc. Perkin Trans. I 1921, 119, 887–891.
- (2). Vermaire DJ; Skaer D; Tippets W A. A. Pract 2019, 12, 103–105. [PubMed: 30052532]
- (3). Schmuhl KK; Gardner SM; Cottrill CB; Bonny AE Subst. Abuse 2019, 1–4.
- (4). Coe MA; Pillitteri JL; Sembower MA; Gerlach KK; Henningfield JE Drug Alcohol. Depend 2019, 202, 24–32. [PubMed: 31284119]
- (5). Buresh M J. Addict. Med 2018, 12, 481–483. [PubMed: 29944481]
- (6). Corkery JM; Streete P; Claridge H; Goodair C; Papanti D; Orsolini L; Schifano F; Sikka K; Korber S; Hendricks A J. Psychopharmacol 2019, 1102–1123. [PubMed: 31429622]
- (7). Murthy P; Clark D Paediatr. Child. Health 2019, 24, 12–14. [PubMed: 30792593]
- (8). Mackay L; Abrahams R Can. Fam. Physician 2018, 64, 121–122. [PubMed: 29449242]
- (9). Cumpston KL; Carter M; Wills BK Am. J. Emerg. Med 2018, 36, 166–168. [PubMed: 28751041]
- (10). Castillo A; Payne JD; Nugent K Proc. (Bayl. Univ. Med. Cent.) 2017, 30, 355–357. [PubMed: 28670086]
- (11). Galbis-Reig D Wmj 2016, 115, 49–52; quiz 53. [PubMed: 27057581]
- (12). Karinen R; Fosen JT; Rogde S; Vindenes V Forensic. Sci. Int 2014, 245, e29–e32. [PubMed: 25453780]
- (13). Forrester MB J. Addict. Dis 2013, 32, 396–400. [PubMed: 24325774]
- (14). Holler JM; Vorce SP; McDonough-Bender PC; Magluilo J Jr.; Solomon CJ; Levine B J. Anal. Toxicol 2011, 35, 54–9. [PubMed: 21219704]
- (15). McWhirter L; Morris S Eur. Addict. Res 2010, 16, 229–31. [PubMed: 20798544]
- (16). The New York Times 4 17, 2019 <https://www.nytimes.com/2019/04/17/us/kratom-overdose-deaths.html> (accessed October 25, 2019)
- (17). U.S. Food & Drug Administration 2 21, 2018 <https://www.fda.gov/news-events/press-announcements/fda-oversees-destruction-and-recall-kratom-products-and-reiterates-its-concerns-risks-associated> (accessed October 25, 2019)
- (18). United States Drug Enforcement Administration 8 30, 2016 <https://www.dea.gov/press-releases/2016/08/30/dea-announces-intent-schedule-kratom> (accessed October 25, 2019)
- (19). Forbes 10 13, 2016 <https://www.forbes.com/sites/davidkroll/2016/08/30/dea-to-place-kratom-mitragynine-on-schedule-i-premature-move-may-compromise-research-benefits/#679fe47d2b8f> (accessed October 25, 2019)
- (20). Johnson EJ; González-Peréz V; Tian D-D; Lin YS; Unadkat JD; Rettie AE; Shen DD; McCune JS; Paine MF Drug Metab. Dispos 2018, 46, 1046–1052. [PubMed: 29735752]
- (21). Tian D-D; Kellogg JJ; Okut N; Oberlies NH; Cech NB; Shen DD; McCune JS; Paine MF Drug Metab. Dispos 2018, 46, 552. [PubMed: 29467215]
- (22). Gufford BT; Chen G; Lazarus P; Graf TN; Oberlies NH; Paine MF Drug Metab. Dispos 2014, 42, 1675–1683. [PubMed: 25008344]
- (23). Kellogg JJ; Paine MF; McCune JS; Oberlies NH; Cech NB Nat. Prod. Rep 2019, 36, 1196–1221. [PubMed: 30681109]

- (24). Brantley SJ; Gufford BT; Dua R; Fediuk DJ; Graf TN; Scarlett YV; Frederick KS; Fisher MB; Oberlies NH; Paine MF CPT: Pharmacometrics Syst. Pharmacol 2014, 3, 107.
- (25). Beckett AH; Shellard EJ; Tackie AN *Planta Med* 1965, 13, 241–246.
- (26). Beckett A; Shellard E; Phillipson J; Lee CM *Planta Med* 1966, 14, 277–288. [PubMed: 5974955]
- (27). Zacharias D; Rosenstein R; Jeffrey G *Acta Crystallogr. A* 1965, 18, 1039–1043.
- (28). Beckett AH; Shellard EJ; Phillipson JD; Lee CM *Planta Med* 1966, 14, 277–288. [PubMed: 5974955]
- (29). Shellard E; Houghton P; Resha M *Planta Med* 1978, 34, 253–263.
- (30). Takayama H; Ishikawa H; Kurihara M; Kitajima M; Aimi N; Ponglux D; Koyama F; Matsumoto K; Moriyama T; Yamamoto LT; Watanabe K; Murayama T; Horie SJ *Med. Chem* 2002, 45, 1949–1956.
- (31). Takayama H *Chem. Pharm. Bull* 2004, 52, 916–928.
- (32). Takayama H; Kitajima M; Kogure N *Curr. Org. Chem* 2005, 9, 1445–1464.
- (33). Marston A; Hostettmann K *Nat. Prod. Rep* 1991, 8, 391–413.
- (34). Stead P, *Isolation by Preparative HPLC In Natural Products Isolation*, Cannell RJP, Ed. Humana Press: Totowa, NJ, 1998; pp 165–208.
- (35). Betz JM; Brown PN; Roman MC *Fitoterapia* 2011, 82, 44–52. [PubMed: 20884340]
- (36). Li S; Yuan W; Deng G; Wang P; Yang P; Aggarwal B *Pharm. Crop* 2011, 2, 28–54.
- (37). Napolitano JG; Lankin DC; Chen SN; Pauli GF *Magn. Reson. Chem* 2012, 50, 569–575. [PubMed: 22730238]
- (38). Niemitz M; Laatikainen R; Chen SN; Kleps R; Kozikowski AP; Pauli GF *Magn. Reson. Chem* 2007, 45, 878–882. [PubMed: 17729231]
- (39). Seebacher W; Simic N; Weis R; Saf R; Kunert O *Magn. Reson. Chem* 2003, 41, 636–638.
- (40). Sy-Cordero AA; Pearce CJ; Oberlies NH *J. Antibiot* 2012, 65, 541–9.
- (41). Kao D; Flores-Bocanegra L; Raja HA; Darveaux BA; Pearce CJ; Oberlies NH *Phytochemistry* 2020, 172, 112238. [PubMed: 31931448]
- (42). <https://www.fda.gov/news-events/public-health-focus/fda-and-kratom> (accessed January 20, 2020)
- (43). Hollingsworth ML; Andra Clark A; Forrest LL; Richardson J; Pennington RT; Long DG; Cowan R; Chase MW; Gaudeul M; Hollingsworth PM *Mol. Ecol. Resour* 2009, 9, 439–457. [PubMed: 21564673]
- (44). Kress WJ; Wurdack KJ; Zimmer EA; Weigt LA; Janzen DH *Proc. Natl. Acad. Sci. USA* 2005, 102, 8369–8374. [PubMed: 15928076]
- (45). Kress WJ; Erickson DL *PLoS one* 2007, 2, e508. [PubMed: 17551588]
- (46). Li X; Yang Y; Henry RJ; Rossetto M; Wang Y; Chen S *Biol. Rev* 2015, 90, 157–166. [PubMed: 24666563]
- (47). Ebihara A; Nitta JH; Ito M *PLoS one* 2010, 5, e15136. [PubMed: 21170336]
- (48). Brown PN; Lund JA; Murch SJ *J. Ethnopharmacol* 2017, 202, 302–325. [PubMed: 28330725]
- (49). Raffa RB, *Kratom and Other Mitragynines: the Chemistry and Pharmacology of Opioids From a Non-opium Source* CRC Press: 2014.
- (50). Takayama H; Kurihara M; Kitajima M; Said IM; Aimi N *Tetrahedron* 1998, 54, 8433–8440.
- (51). León F; Habib E; Adkins JE; Furr EB; McCurdy CR; Cutler SJ *Nat. Prod. Commun* 2009, 4, 907–910. [PubMed: 19731590]
- (52). Beckett A; Shellard E; Phillipson J; Lee CM *J. Pharm. Pharmacol* 1965, 17, 753–755. [PubMed: 4379809]
- (53). Shellard EJ; Houghton PJ; Resha M *Planta Med* 1978, 33, 223–227.
- (54). Cao X-F; Wang J-S; Wang X-B; Luo J; Wang H-Y; Kong L-Y *Phytochemistry* 2013, 96, 389–396. [PubMed: 24169379]
- (55). Beckett AH; Lee CM; Tackie AN *Tetrahedron Lett* 1963, 4, 1709–1714.
- (56). Hemingway SR; Houghton PJ; Phillipson JD; Shellard EJ *Phytochemistry* 1975, 14, 557–563.
- (57). Ali Z; Demiray H; Khan IA *Tetrahedron Lett* 2014, 55, 369–372.

- (58). Cu N Bull. Soc. Chim. Fr 1957, 1292–1294.
- (59). Shellard E *Planta Med* 1978, 34, 26–36.
- (60). Kitajima M; Misawa K; Kogure N; Said IM; Horie S; Hatori Y; Murayama T; Takayama H J. *Nat. Med* 2006, 60, 28–35.
- (61). Lee CM; Trager WF; Beckett AH *Tetrahedron* 1967, 23, 375–385. [PubMed: 6037287]
- (62). 1H NMR Properties of Piperidine Derivatives In *Studies in Organic Chemistry*, Rubiralta M; Giralt E; Diez A, Eds. Elsevier: 1991; Vol. 43, pp 34–87.
- (63). Alkorta I; Elguero J *Magn. Reson. Chem* 2004, 42, 955–961. [PubMed: 15386552]
- (64). Trager W; Lee CM; Phillipson J; Haddock R; Dwuma-Badu D; Beckett A *Tetrahedron* 1968, 24, 523–543. [PubMed: 5637484]
- (65). Xu J; Shao L-D; Li D; Deng X; Liu Y-C; Zhao Q-S; Xia C J. *Am. Chem. Soc* 2014, 136, 17962–17965. [PubMed: 25496352]
- (66). Berner M; Tolvanen A; Jokela R, *Acid-catalysed Epimerization of Bioactive Indole Alkaloids and Their Derivatives In Studies in Natural Products Chemistry*, Atta ur R, Ed. Elsevier: 2001; Vol. 25, pp 3–42.
- (67). Laus G; Wurst K *Helv. Chim. Acta* 2003, 86, 181–187.
- (68). Wanner MJ; Ingemann S; van Maarseveen JH; Hiemstra H *Eur. J. Org. Chem* 2013, 2013, 1100–1106.
- (69). Reinhardt JK; Klemd AM; Danton O; De Mieri M; Smieško M; Huber R; Bürgi T; Gründemann C; Hamburger M J. *Nat. Prod* 2019, 82, 1424–1433. [PubMed: 31181920]
- (70). Bustos-Brito C; Joseph-Nathan P; Burgueño-Tapia E; Martínez-Otero D; Nieto-Camacho A; Calzada F; Yépez-Mulia L; Esquivel B; Quijano L J. *Nat. Prod* 2019, 82, 1207–1216. [PubMed: 31063376]
- (71). El-Kashef DH; Daletos G; Plenker M; Hartmann R; Mándi A; Kurtán T; Weber H; Lin W; Ancheeva E; Proksch P J. *Nat. Prod* 2019, 82, 2460–2469. [PubMed: 31432669]
- (72). Cao F; Meng Z-H; Mu X; Yue Y-F; Zhu H-J J. *Nat. Prod* 2019, 82, 386–392. [PubMed: 30724084]
- (73). Arreaga-González HM; Rodríguez-García G; del Río RE; Ferreira-Sereno JA; García-Gutiérrez HA; Cerda-García-Rojas CM; Joseph-Nathan P; Gómez-Hurtado MA J. *Nat. Prod* 2019, 82, 3394–3400. [PubMed: 31751133]
- (74). Raja HA; Baker TR; Little JG; Oberlies NH *Food Chem* 2017, 214, 383–392. [PubMed: 27507489]
- (75). Dunning LT; Savolainen V J. *Linn. Soc., Bot* 2010, 164, 1–9.
- (76). Ford CS; Ayres KL; Toomey N; Haider N; Van Alphen Stahl J; Kelly LJ; Wikström N; Hollingsworth PM; Duff RJ; Hoot SB J. *Linn. Soc., Bot* 2009, 159, 1–11.
- (77). Pawar RS; Handy SM; Cheng R; Shyong N; Grundel E *Planta Med* 2017, 83, 921–936. [PubMed: 28454189]
- (78). Cheng T; Xu C; Lei L; Li C; Zhang Y; Zhou S *Mol. Ecol. Resour* 2016, 16, 138–149. [PubMed: 26084789]
- (79). Löfstrand SD; Krüger Å; Razafimandimbison SG; Bremer B *Syst. Bot* 2014, 39, 304–315.
- (80). Razafimandimbison SG; Bremer B *Am. J. Bot* 2002, 89, 1027–1041. [PubMed: 21665704]
- (81). Tnah L; Lee S; Tan A; Lee C; Ng K; Ng C; Farhanah ZN *Food Control* 2019, 95, 318–326.
- (82). Raja HA; Miller AN; Pearce CJ; Oberlies NH J. *Nat. Prod* 2017, 80, 756–770. [PubMed: 28199101]

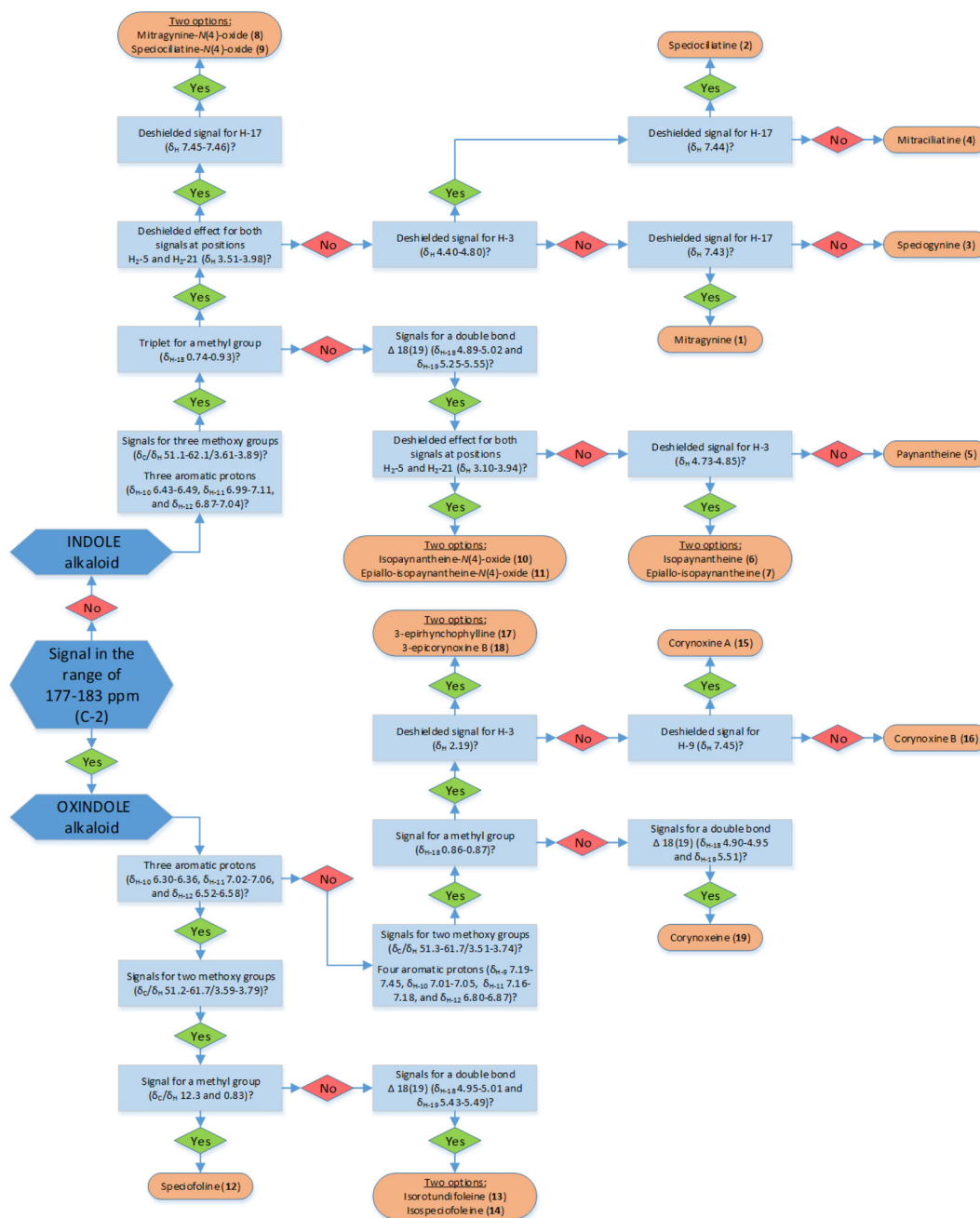


Figure 1.

Decision tree for differentiating between **1-19** based on key NMR signals. As a single starting point, the ^{13}C NMR signal for the lactam moiety is used to distinguish between oxindole (present) or indole (absent) kratom alkaloids. Once the broad structural class is determined, ^1H NMR data can be used via a flowchart as a guide to elucidate the structure of these alkaloids.

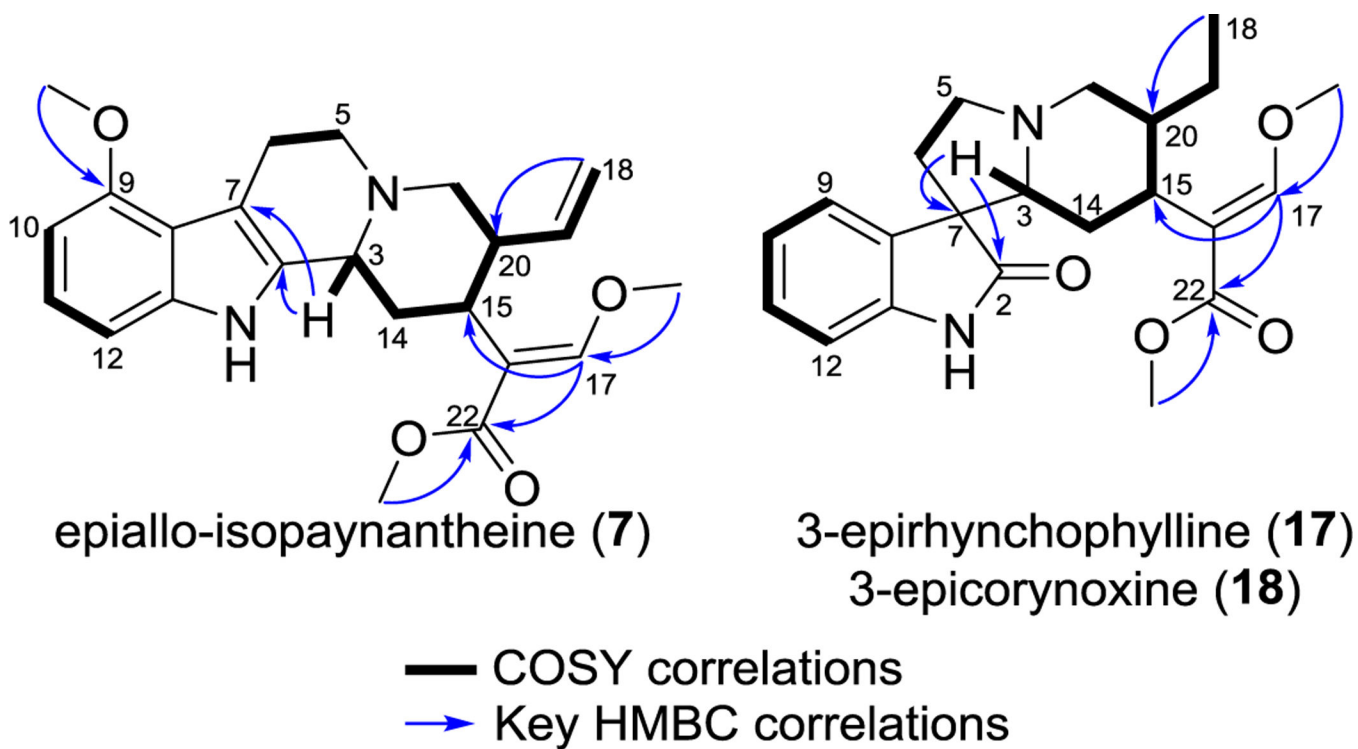


Figure 2.
Key correlations observed in the COSY and HMBC spectra for compounds **7**, **17**, and **18**.
The latter two have the same 2D structure and thus the same correlations.

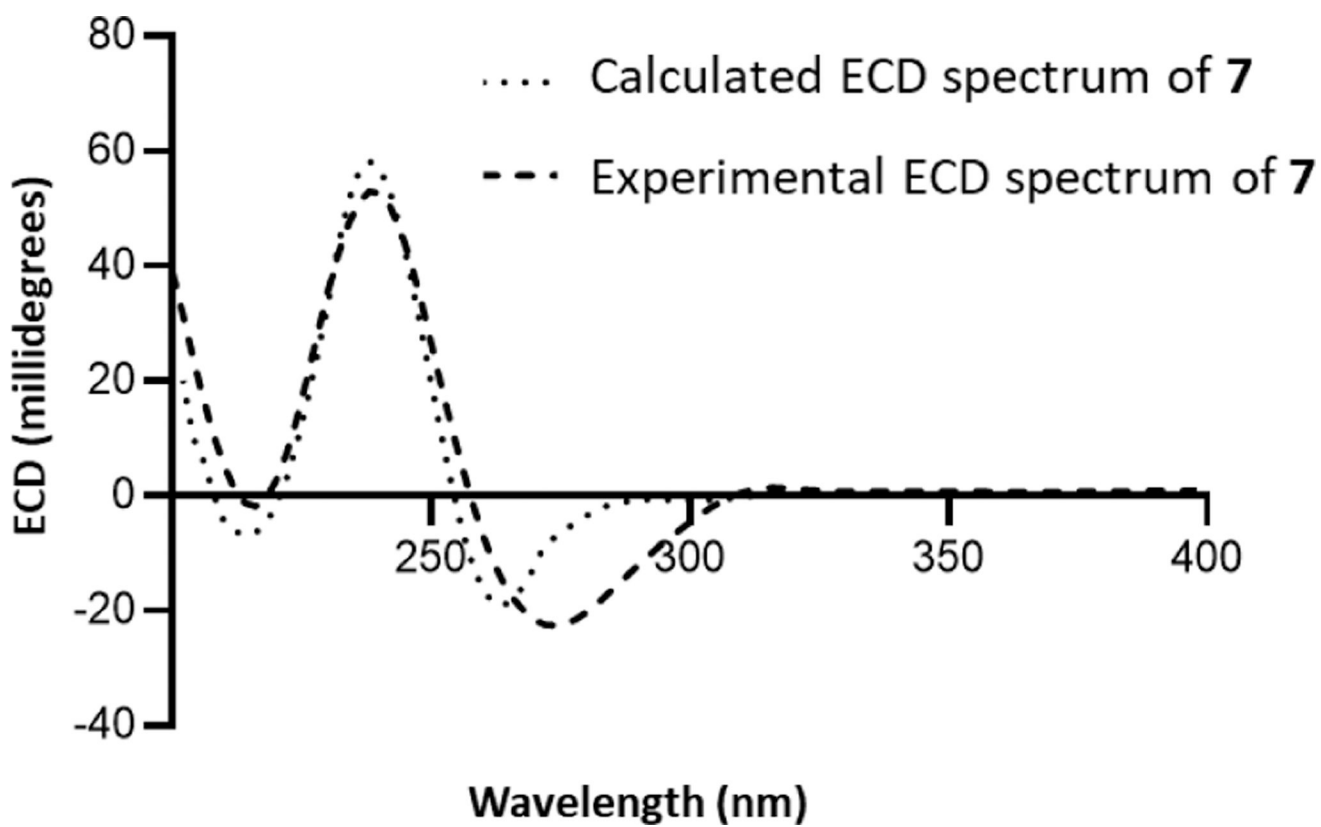


Figure 3. Experimental ECD spectrum of **7** in CH₃OH at 0.2 mg/mL (dashed line) and calculated ECD spectrum of (3*R*,15*S*,20*S*)-**7** (dotted line).

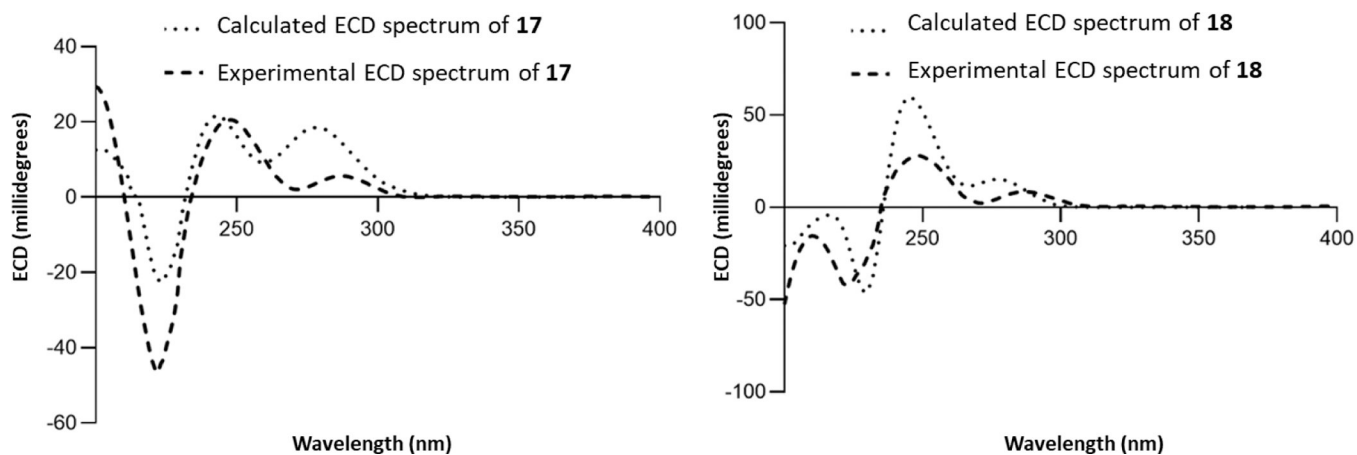


Figure 4.

A) Experimental ECD spectra of **17** in CH₃OH at 0.2 mg/mL (dashed lines) and calculated ECD spectrum of (3*R*,7*R*,15*S*,20*R*)-**17** (dotted lines). B) Experimental ECD spectra of **18** in CH₃OH at 0.2 mg/mL (dashed lines) and calculated ECD spectrum of (3*R*,7*R*,15*S*,20*S*)-**18** (dotted lines).

Table 1.

Characteristic ^1H and ^{13}C NMR Data for Compounds 1–4 (CDCl_3 , 400 and 100 MHz, Respectively)^a

position	mitragynine (1)		speciociliatine (2)		speciogymine (3)		mitraciliatine (4)	
	δ_{C}	δ_{H} (J in Hz)	δ_{C}	δ_{H} (J in Hz)	δ_{C}	δ_{H} (J in Hz)	δ_{C}	δ_{H} (J in Hz)
3	61.3	CH 3.20, d (8.4)	54.7	CH 4.40, bs	61.9	CH 3.21, m	53.9	CH 4.80, s
10	99.9	CH 6.45, d (7.7)	99.8	CH 6.47, d (7.7)	99.8	CH 6.44, d (7.8)	99.7	CH 6.49, d (7.6)
11	122.0	CH 7.00, t (7.9)	122.4	CH 7.02, t (8.0)	122.4	CH 6.99, t (7.9)	122.6	CH 7.07, t (7.9)
12	104.3	CH 6.90, d (8.1)	104.5	CH 6.91, d (8.1)	104.5	CH 6.87, d (8.0)	104.9	CH 7.01, d (8.0)
17	160.7	CH 7.43, s	160.6	CH 7.44, s	160.4	CH 7.35, bs	160.2	CH 7.32, s
18	13.0	CH_3 0.87, t (7.3)	12.5	CH_3 0.89, t (7.9)	11.1	CH_3 0.85, t (7.2)	11.1	CH_3 0.74, t (7.0)
9-OCH ₃	55.5	CH_3 3.87, s	55.3	CH_3 3.88, s	55.4	CH_3 3.85, s	55.3	CH_3 3.89, s
17-OCH ₃	61.7	CH_3 3.73, s	61.7	CH_3 3.78, s	61.9	CH_3 3.72, s	61.8	CH_3 3.77, s
22-OCH ₃	51.5	CH_3 3.71, s	51.6	CH_3 3.66, s	51.1	CH_3 3.72, s	51.5	CH_3 3.68, s
NH		7.74, bs		8.00, bs		7.94, bs		8.98, bs

^aSee Table S4 for a full comparison for the ^1H and ^{13}C NMR data for 1–4 (Supporting Information).

Table 2.

Characteristic ^1H and ^{13}C NMR Data for Compounds 5–7 (CDCl_3 , 400 and 100 MHz, Respectively)^a

Position	paynantheine (5)			isopaynantheine (6)			epiallo-isopaynantheine (7)		
	δ_{C}	type	δ_{H} (J in Hz)	δ_{C}	type	δ_{H} (J in Hz)	δ_{C}	type	δ_{H} (J in Hz)
3	60.1	CH	3.20, m	53.8	CH	4.73, bs	53.9	CH	4.85, bs
10	99.9	CH	6.45, d (7.8)	99.7	CH	6.49, d (7.6)	99.7	CH	6.49, d (7.8)
11	122.1	CH	7.00, t (7.9)	122.6	CH	7.07, t (7.9)	122.9	CH	7.08, t (7.9)
12	104.3	CH	6.88, d (8.0)	105.0	CH	7.02, d (8.1)	105.0	CH	7.01, d (8.1)
17	160.0	CH	7.33, s	160.2	CH	7.28, s	160.3	CH	7.28, s
18	115.7	CH ₂	5.01, dd (17.3, 2.0) 4.96, dd (10.4, 2.1)	116.7	CH ₂	4.96, dd (17.2, 1.8) 4.89, dd (10.2, 1.8)	117.2	CH ₂	4.98, dd (17.3, 1.7) 4.91, dd (10.3, 1.8)
19	139.4	CH	5.55, dt (17.9, 9.3)	137.9	CH	5.29, ddd (18.0, 10.3, 8.3)	137.1	CH	5.27, ddd (18.0, 10.3, 8.3)
9-OCH ₃	55.4	CH ₃	3.88, s	55.3	CH ₃	3.89, s	55.3	CH ₃	3.88, s
17-OCH ₃	61.7	CH ₃	3.78, s	61.7	CH ₃	3.76, s	61.7	CH ₃	3.76, s
22-OCH ₃	51.5	CH ₃	3.69, s	51.4	CH ₃	3.67, s	51.5	CH ₃	3.67, s
NH			7.85, s			8.91, s			9.12, s

^aSee Table S5 for a full comparison for the ^1H and ^{13}C NMR data for 5–7 (Supporting Information).

Table 3.

Characteristic ^1H and ^{13}C NMR Data for Compounds 8–11 (CDCl_3 , 400 and 100 MHz, Respectively)^a

position	mitragynine-N(4)-oxide (8)		speciociliatine-N(4)-oxide (9)		isopaynantheine-N(4)-oxide (10)		epiallo-isopaynantheine-N(4)-oxide (11)	
	δ_{C}	δ_{H} (J in Hz)	δ_{C}	type	δ_{H} (J in Hz)	δ_{C}	type	δ_{H} (J in Hz)
3	66.9	CH	5.16, s	CH	5.04, d (12.5)	69.2	CH	5.04, bs
10	99.7	CH	6.43, d (7.7)	CH	6.43, d (7.7)	99.9	CH	6.49, d (7.8)
11	123.3	CH	7.03, t (7.9)	CH	6.99, t (7.9)	123.8	CH	7.11, t (7.9)
12	105.2	CH	6.95, d (8.1)	CH	6.92, bs	105.1	CH	7.03, d (8.2)
17	161.5	CH	7.45, s	CH	7.46, s	160.5	CH	7.31, s
18	12.7	CH ₃	0.93, t (7.2)	CH ₃	0.85, t (7.4)	118.0	CH ₂	5.02, dd (17.5, 1.0) 4.95, dd (10.2, 1.7)
9-OCH ₃	55.2	CH ₃	3.85, s	CH ₃	3.86, s	55.3	CH ₃	3.88, s
17-OCH ₃	62.1	CH ₃	3.80, s	CH ₃	3.85, s	62.0	CH ₃	3.80, s
22-OCH ₃	51.6	CH ₃	3.61, s	CH ₃	3.68, s	51.6	CH ₃	3.68, s
NH			9.46, s	-	-			8.84, s

^aSee Table S6 for a full comparison for the ^1H and ^{13}C NMR data for 8–11 (Supporting Information).

Table 4.

Characteristic ^1H and ^{13}C NMR Data for Compounds 12–14 (CDCl_3 , 500 and 125 MHz, Respectively)^a

Position	speciofoline (12)		isorotundifoline (13)		isospiciofoline (14)	
	δ_{C}	δ_{H} (J in Hz)	δ_{C}	δ_{H} (J in Hz)	δ_{C}	δ_{H} (J in Hz)
2	180.2	C	177.7	C	179.1	C
3	63.8	CH	66.6	CH	68.7	CH
7	57.3	C	55.9	C	57.5	C
9	154.6	C	155.1	C	154.6	C
10	111.9	CH	112.1	CH	111.4	CH
11	129.6	CH	129.2	CH	129.6	CH
12	101.1	CH	100.3	CH	101.0	CH
17	159.8	CH	159.8	CH	159.9	CH
18	12.3	CH_3	116.4	CH_2	116.4	CH_2
19	24.2	CH_2	138.8	CH	138.6	CH
17- OCH_3	61.3	CH_3	61.7	CH_3	61.5	CH_3
22- OCH_3	51.7	CH_3	51.3	CH_3	51.2	CH_3
NH			8.44, s	7.45, s		7.60, s

^aSee Table S7 for a full comparison for the ^1H and ^{13}C NMR data for 12-14 (Supporting Information).

Table 5.

Characteristic ^1H and ^{13}C NMR Data for Compounds 15–19 (CDCl_3 , 500 and 125 MHz, Respectively)^a

position	corynoxine A (15)		corynoxine B (16)		3-epirhynchophylline (17)		3-epicorynoxine B (18)		corynoxine (19)		
	δ_{C}	δ_{H} (J in Hz)	δ_{C}	type	δ_{H} (J in Hz)	type	δ_{C}	type	δ_{C}	type	δ_{H} (J in Hz)
2	182.4	C	182.3	C	181.2	C	182.2	C	181.0	C	
3	73.2	CH	76.5	CH	77.4	CH	77.0	CH	75.2	CH	2.30, dd (11.3, 2.5)
9	125.0	CH	123.2	CH	123.3	CH	123.4	CH	123.5	CH	7.22, d (7.8)
10	122.5	CH	122.5	CH	122.5	CH	122.9	CH	122.7	CH	7.05, td (7.6, 1.0)
11	127.4	CH	127.9	CH	127.8	CH	128.1	CH	128.0	CH	7.18, td (7.7, 1.2)
12	109.5	CH	109.5	CH	109.1	CH	109.6	CH	109.2	CH	6.82, d (7.7)
18	13.0	CH ₃	13.4	CH ₃	13.5	CH ₃	13.3	CH ₃	115.6	CH ₂	4.95, ddd (17.2, 2.01, 0.8) 4.90, dd (10.2, 2.1)
19	19.4	CH ₂	19.3	CH ₂	19.3	CH ₂	19.8	CH ₂	139.6	CH	5.51, dt (18.0, 9.1)
17-OCH ₃	61.2	CH ₃	61.6	CH ₃	61.7	CH ₃	61.7	CH ₃	61.7	CH ₃	3.74, s
22-OCH ₃	51.3	CH ₃	51.4	CH ₃	51.4	CH ₃	51.4	CH ₃	51.4	CH ₃	3.62, s
NH			8.40, s		8.91, s		7.62, s		7.33, s		7.53, s

^aSee Table S8 for a full comparison for the ^1H and ^{13}C NMR data for 15–19 (Supporting Information).